Analytical Methods

Accepted Manuscript

This is an *Accepted Manuscript*, which has been through the RSC Publishing peer review process and has been accepted for publication.

Accepted Manuscripts are published online shortly after acceptance, which is prior to technical editing, formatting and proof reading. This free service from RSC Publishing allows authors to make their results available to the community, in citable form, before publication of the edited article. This *Accepted Manuscript* will be replaced by the edited and formatted *Advance Article* as soon as this is available.

To cite this manuscript please use its permanent Digital Object Identifier (DOI®), which is identical for all formats of publication.

More information about *Accepted Manuscripts* can be found in the **Information for Authors**.

Please note that technical editing may introduce minor changes to the text and/or graphics contained in the manuscript submitted by the author(s) which may alter content, and that the standard **Terms & Conditions** and the **ethical guidelines** that apply to the journal are still applicable. In no event shall the RSC be held responsible for any errors or omissions in these *Accepted Manuscript* manuscripts or any consequences arising from the use of any information contained in them.

Application of 3-D Surface Reconstruction by Mid- and Near-Infrared Microscopic Imaging for Anatomical Studies on *Hericium coralloides* Basidiomata

J. D. Pallua[1,7], S. H. Unterberger[2], G. Metzler[2], K. Pfaller[3], A. K. Pallua[4], R. Lackner[2], A. F. Pallua[5], W. Recheis[6] and R. Pöder[7]

[1]Institute of Legal Medicine, Medical University of Innsbruck, Müllerstraße 44, 6020 Innsbruck, Austria

[2]Material-Technology, Leopold-Franzens University Innsbruck, Technikerstraße 13, 6020 Innsbruck, Austria

[3]Section for Histology and Embryology, Medical University of Innsbruck, Müllerstraße 59, 6020 Innsbruck, Austria

[4] Former Institute for Computed Tomography-Neuro CT, Medical University of Innsbruck, Anichstraße 35, 6020 Innsbruck, Austria

[5]Section for Clinical Neurobiology, Medical University of Innsbruck, Anichstraße 35, 6020 Innsbruck, Austria

[6]Department of Radiology, Medical University of Innsbruck, Anichstraße 35, 6020 Innsbruck, Austria

[7]Institute of Microbiology, Leopold-Franzens University, Technikerstraße 25, 6020 Innsbruck, Austria

Correspondence address:

MMag. Dr. Johannes Pallua, Institute of Microbiology, Leopold-Franzens University, Technikerstraße 25, 6020 Innsbruck, Austria, Institute of Legal Medicine, Medical University of Innsbruck, Müllerstraße 44, 6020 Innsbruck, Austria

Johannes.Pallua@i-med.ac.at

Abbreviations

Charge coupled device (CCD), hierarchical cluster analysis (HCA), infrared (IR), Fourier transform infrared (FTIR), fresh weight (FW), fuzzy C-means (FCM), K-means clustering (KMC), mid infrared (MIR), multivariate imaging analysis (MIAs), mercury cadmium telluride (MCT), near infrared (NIR), principle component analyses (PCA), three-dimensional (3-D), regions of interest (ROIs), Traditional Chinese Medicine (TCM)

Abstract

Tens of thousands of known mushrooms (incl. mycelia) represent, beside their nutritional and economic value, a huge reservoir of biological active substances. A growing list of publications reports beneficial or therapeutic health effects (e.g., immunomodulatory, lipid-lowering, and antitumor properties) of so called “medicinal mushrooms”. Their potential pharmacological properties, however, were not or still not sufficiently investigated. Therefore, any novel approach that improves our knowledge on the medicinal relevance, as well as quality control in the cultivation of medicinal mushrooms, should be welcome.

In the present study, 3-D surface mid-infrared (MIR) and near-infrared (NIR) microscopic imaging as well as data analysis methods were combined to study 3-D molecular patterns of the edible and potentially medicinal basidiomycete *Hericium coralloides*. For 3-D surface measurements, spectral images from different planes within the surface layer of the mushroom were acquired. We tested several evaluation processes and optimized the methodology for use of complex infrared images to monitor 3-D molecular patterns in fruiting body (basidioma) structures. It is demonstrated that 3-D surface MIR and NIR microscopic imaging enables to gain a picture of the semi-quantitative distribution/location of defined substance classes within the fruiting body. Such analyses might be useful for quality and safety control in the production and consumption of medicinal mushrooms.

1. Introduction

Fungi represent, concerning their number and species diversity, according to insects the second largest taxonomic group of organisms on Earth and are far from being thoroughly investigated. By now, more than 120000 species are known and annually 1800 new species of fungi are described. According to current estimates, at least 1.5 million species of fungi exist [1, 2]. In many respects the level of knowledge of already identified species is incomplete, in which their potential pharmacological properties is insufficiently investigated [3-5]. So far, it is believed that only 16 % of the described species have (partly) been studied biochemically [4].

Natural products from fungi possess a promising potential in the development of new drugs as well as in the search for environmentally friendly herbicides. Of particular benefit is the ability of fungi to produce a variety of secondary metabolites, which – in contrast to primary metabolites – are not considered to take a central role in energy production or cell structure. Fungal secondary metabolites rather serve as scents and attractants or even as defence mechanism against bacteria, viruses, insects, and competing-generating fungi, in which several of these secondary metabolites are used as major drugs or herbicides [6]. Among the well-studied fungi – mostly anamorphic Ascomycota and Basidiomycota – there are a few that have turned out to be essential in human medicine (cf. penicillin from Penicillium chrysogenum Thom [7-9], cyclosporine from Elaphocordyceps subsessilis (Petch) G.H. Sung, J.M. Sung & Spatafora (= Tolypocladium inflatum W. Gams) [10, 11], mevinolin from Aspergillus terreus Thom [12, 13] or Pleurotus ostreatus (Jacq.) P. Kumm. [14-16], taxol from Taxomyces andreanae Strobel, A. Stierle, D. Stierle & W.M. Hess [17, 18] and asperlicin from Aspergillus alliaceus Thom & Church [19-22]). The variety of chemical compounds that have been detected or isolated from fungi so far leads one to suspect that an enormous potential of pharmacological and biomedical research is still available. Hence, more information about bioactive fungal ingredients – in particular on metabolites of cultivable fungi – is welcome in order to assess their relevance to medicine, as well as to improve their harvesting time and culture quality [23-28]. Consequently, a characterization of chemical components and structure-function relationships is desirable and promising. So far, the relatively few mushrooms studied represent a vast source of biologically active ingredients, and therefore, among

other scientific issues, a deeper characterization of structure–function relationships and chemical components is still desirable.

In this study, the application of three-dimensional (3-D) surface mid-infrared (MIR) and near-infrared (NIR) microscopic imaging is linked with data analysis methods in order to get a deeper insight into structure-function relationships in the potentially medicinal and edible fungus *Hericium coralloides* (Scop.) Pers. (Basidiomycota, Agaricomycotina).

Hericium fruiting bodies (basidiomata, 'mushrooms') or mycelia have long been used in Traditional Chinese Medicine (TCM) to treat various diseases. Especially *Hericium erinaceus*, which is taxonomically closely related to *H. coralloides*, has attracted great attention due to its antimicrobial effect, anti-tumour immunomodulatory and lipid-lowering activities, antioxidant properties, cytotoxic effect, the promotion of synthesis of neurogrowth factors [29] as well as the prevention of dementia [30]. For that reason more information about members of the genus Hericium is welcome to evaluate the efficiency of its representatives and strains, also to improve mushroom yield and quality.

3-D images of basidiomata (fruiting bodies) or tissue specimens are extremely useful to investigate such relationships. Conventional ways of generating such 3-D images are computed tomography (CT), positron emission tomography (PET), and magnetic resonance imaging (MRI), even if they have been rarely used for structural analysis of fungal tissues. These methods, however, lack of information about the macromolecular composition in the image contrast. Hence molecular imaging would provide a useful and novel alternative to the conventional ways with the advantage of image contrast based directly on the underlying macromolecular composition. The drawback of molecular imaging is the surface sampling mode, precluding real time imaging of whole samples. An alternative is to build a composite from 2-D images of adjacent sections or Z coordinates of a sample to get 3-D information[31, 32]. Regrettably, the available knowledge in this field is extremely sparse to date. Only few reports of 3-D infrared (IR) microscopic imaging [33-36] are known. Thus, 3-D surface layer MIR and NIR microscopic imaging was achieved by reconstruction of 2-D spectral images from different planes within the surface layer of a *Hericium coralloides* basidioma. IR microscopic imaging is now regarded as attractive and promising analytical tool for environmental mapping [37], precision farming [38], food quality evaluation [39], product functionality [40, 41], determining the severity of plant diseases [42, 43], detecting defects [44] and contaminations [45-47], determining the distribution of certain chemical components [48-52] as

well as detection and characterization of human malignancies in several tissues [53-67]. In this study, MIR and NIR microscopic imaging is applied on a *Hericium coralloides* basidioma to develop new tools for histo-anatomical analyses of fungal tissues and to study the distribution of certain bio-molecules. Because 3-D surface MIR and NIR microscopic imaging has not been applied until now to study fungal tissues, an important goal of this study was to optimize measurement parameters and data analysis. To understand the signals of the basidiome surface planes, the analysis of the spatial distribution of chemical constituents in the fungal surface layers, which include the basidia as reproductive cells, is of prime importance. On that account, a combined 3-D surface analysis based on 2-D spectral images acquired from different tissue planes and 3-D surface rendering of the MIR and NIR dataset was developed. Several algorithms for spectral interpretation were evaluated. Finally, the efficiency of this 3-D approach to get novel insights into the anatomy and the location/distribution of chemical substance classes in the basidiome is demonstrated and discussed. A schematic diagram of the work flow is presented in **Fig. 1**.

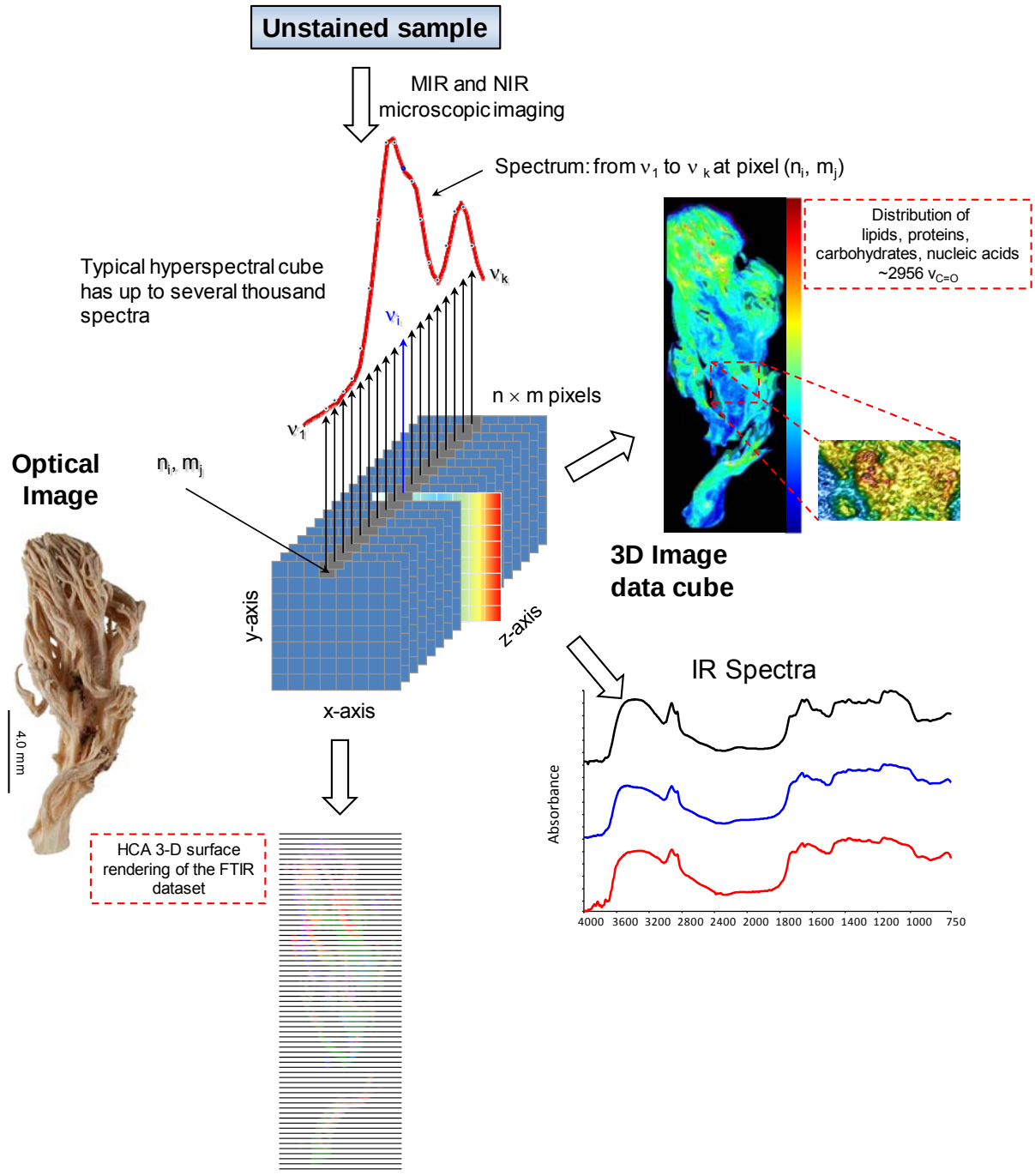

Figure 1 Overview of the application of 3-D surface MIR and NIR microscopic imaging to the medicinal fungus *Hericium coralloides*. A dried and unstained basidiome sample is analysed by MIR and NIR microscopic imaging to get a spatial distribution of different biomolecules (e.g., DNA, proteins, peptides, lipids). A parallel taken photo of the specimen will be used to assign the different anatomical structures of the sample by a mycologist. Overlay of all datasets will allow a 3-D assignment of biomolecules to the different anatomical structures.

2 Material and Methods

2.1 Tissue Preparation

Hericium coralloides basidiomes collected in a local forest near Innsbruck was used for this study. Voucher material is deposited in the Mycological Collection of the Herbarium of the University of Innsbruck (IB 20060500). One specimen from a fresh basidioma (319.77 mg FW) including different orders of side branches was fixed with 3 % formaldehyde. After fixation the specimen was critical-point dried (36.99 mg). The dried specimen (dimensions: x-axis 171.0 mm, y-axis 6.2 mm, and z-axis 3.4 mm) was photographed for anatomical reevaluation and comparison to the imaging results.

2.2 3-D Surface MIR and NIR Microscopic Imaging

Mid infrared (MIR) and near infrared (NIR) reflection measurements were performed at room temperature using a Bruker Vertex 70 Fourier transform infrared (FTIR) spectrometer, which was continuously flushed with dried air to minimize water-vapor background, coupled to a Hyperion 3000 microscope equipped with a usual nitrogen-cooled MCT-D316-025 (mercury cadmium telluride) detector called single-element detector and a nitrogen-cooled focal plane array (FPA) detector consisting of 64 × 64 MCT-D364 detectors. Visual image collection was done via a charge coupled device (CCD) camera integrated in the microscope stage motion and IR data acquisition.

The specimen was measured with a nominal lateral resolution of 50 µm × 50 µm per pixel for each spot by mapping using a conventional MCT detector. MIR (detector range set from 4000 cm^{-1} to 750 cm^{-1}) and NIR (detector range set from 7800 cm^{-1} to 4000 cm^{-1}) spectra were recorded with a spectral resolution of 8 cm^{-1} with 16 co-added scans from a total imaged area of 6200 µm × 17100 µm. Before each sample measurement, background spectrum of a gold-coated substrate was recorded with a spectral resolution of 8 cm^{-1} with 105 co-added scans to subtract the reference spectrum from the dataset automatically. Scan rate and resolution were optimized to get a good signal to noise ratio of the recorded spectra. For detailed information about detector theory, technology and current developments the interested reader is referred to the cited literature [31, 32, 68].

To build a 3-D surface image, six image planes (500 µm in distance) were scanned, including the full range of features in the specimen under study. In this way 6 IR images were generated, capturing the spectral variation of the fungal surface.

2.3 Data Processing

All spectral data processing and image assembling were performed using OPUS 6.5 software (Bruker), The Unscrambler X 10.2 (Camo, Norway, Oslo) and CytoSpec^{TM} software package (www.cytospec.com, Hamburg, Germany). 3-D univariate chemical maps depicting a single spectral feature and multivariate imaging analysis (MIAs) were generated by using CytoSpec^{TM} software, Fiji (http://fiji.sc/Fiji) and Amira 5.3.3 (Visage Imaging, Richmond, Australia).

Principle component analyses (PCA)

Before principle component analyses (PCA) and image analysis it was necessary to remove atmospheric absorptions and noise by using OPUS 6.5 software (Bruker).

PCA models were generated with The Unscrambler X 10.2 software, after atmospheric correction and noise reduction. For PCA model generation, tissue type-associated spectra were selected using the CytoSpecTM software. For this purpose, we evaluated the sample and defined the regions of interest (ROIs). Extracted spectra of ROIs were imported into The Unscrambler X 10.2 software and underwent several data pretreatments (e.g., baseline correction, normalization), before PCA model generation.

2-D MIR and NIR image analysis

For univariate image analysis as well as MIAs, 2-D IR images were loaded in the CytoSpec software. Spectral quality test was performed to eliminate spectra from areas with poor signal to noise ratio or without tissue. So, for further processing, a 400 for the minimal and 700 for maximal integrated intensity criterion in the wavenumber range of 5000 cm^{-1} to 5330 cm^{-1} was set. Remaining spectra were vector-normalized and smoothed (Savitzky-Gloay, 13 smoothing points) in the wave number range 7600 cm^{-1} to 750 cm^{-1} before univariate image analysis. These procedures lead to higher resolved peaks, eliminated background slopes and reduced influence of intensity changes caused by differences in

tissue density and roughness of the tissue [69]. The processed spectral datasets were used for subsequent univariate image analyses and MIAs.

MIAs such as hierarchical clustering (HCA), k-means (KMC) clustering and fuzzy C-means clustering (FCM) in the spectral ranges 6000 cm^{-1} to 4200 cm^{-1}, 3000 cm^{-1} to 2800 cm^{-1} and 1800 cm^{-1} to 850 cm^{-1} (fingerprint region) were used for data analyses. For detailed information about univariate image analysis as well as MIAs theory and current developments the interested reader is referred to the cited literature [31, 61, 70-77].

3-D reconstruction of 2-D univariate and 2-D MIAs images

3-D univariate and MIAs models of the surface are constructed from the stack of images, calculating x, y, and z coordinates for any point within the resolution of the scan, allowing the reconstruction based on the underlying bio-chemistry. The 3-D univariate and MIAs maps were rendered from a scalar volume field of absorbance values generated from 2-D IR images stacked in Fiji and Amira. Furthermore, 3-D univariate maps and 3-D pseudo-colour cluster images of MIAs were assembled and compared directly with the optical images captured from the same sample. The different clustering techniques were used to find out which method is the best to reproduce the actual morphology and the accumulation of different ingredients. The use of any of the clustering algorithms increased the information content of the IR images, as compared to univariate methods, and several authors employed multivariate pattern recognition methods such as principal component analysis [78, 79], agglomerative hierarchical (AH) clustering [80-82], k-means and fuzzy C-means (KM, FCM) clustering [83, 84].

3 Results and Discussion

Analysis of the resulting data set by spectra analysis, principal component analysis (PCA), 3-D surface chemical maps and 3-D pseudo-colour cluster images are illustrated in **Figs. 2-4**. **Fig. 2 (A)-(B)** display typical MIR (detector range set from 4000 cm^{-1} to 750 cm^{-1}) and NIR (detector range set from 7600 cm^{-1} to 4000 cm^{-1}) spectra of the most basal branch (black), subsequent lateral branch (blue), and end-branch (red) regions obtained from a randomly selected part of the upper region of a fresh *H. coralloides* basidioma.

Prominent spectral features in spectra of all mentioned basidioma regions are the first overtone of O-H deformation and C-H stretching at 4755 cm^{-1}, the protein amide A vibration at approximately 3300 cm^{-1}, the C-H stretching vibrations of phospholipids, of protein side chains, nucleic acid sugars, complex carbohydrates as well as that of amorphous or fully hydrated sugars between 3000 cm^{-1} and 2800 cm^{-1}, the C-H deformation modes and some carboxylic acid modes between 1450 cm^{-1} and 1350 cm^{-1}, and carbohydrate bands, which occur at 1185 cm^{-1}. The less resolved, broader bands in the carbohydrate region might arise from amorphous simple sugars and/or polysaccharides like chitin and β-glucans. In fungal cells, these chemical components are often produced in high amounts [51, 85].

Highly absorbing compounds in the basal branch region are phosphate groups of DNA, RNA as well as some phospholipids (absorption at 1240 cm^{-1}), amide-II proteins with high tyrosine content (absorption at 1515 cm^{-1}), amide-II proteins (absorption at 1550 cm^{-1}), and amide-I proteins (absorption at 1630 cm^{-1}, considered as relevant marker for both peptide and protein secondary structure). These observations clearly indicate that this anatomical substructure features a high protein production rate.

It was observed that highly absorbing compounds in side branch regions were: $\nu_{C\text{-}O\text{-}C}$ symmetric vibrations at 1060 cm^{-1} of phospholipids, cholesterols, esters, and $\nu_{P=O}$ symmetric vibrations at 1084 cm^{-1} of the $>PO_2^-$ groups of nucleic acids and phospholipids. Symmetric phosphate as discriminating spectral marker was first proposed as a feature of stem cells by Walsh MJ et al [86]; this group later presented a distribution of this spectral marker associated with cancer stem cells [87]. In our study, this spectral marker is highly absorbing in tissues of

basidioma side branches, indicating that they are strongly proliferating during basidiomatal development.

End branch regions exhibit a high absorption at 1038 cm^{-1} (ν_{C-O} carbohydrates), at 1740 cm^{-1} ($\nu_{C=O}$ esters, phospholipids as well as carbohydrates), at 4332 cm^{-1} (C-H stretching and deformation combination), at 5175 cm^{-1} (O-H stretching and deformation vibration, H_2O, polysaccharides), and at 5796 cm^{-1} (first overtone of C-H stretching), suggesting that this end branches produce high amounts of carbohydrates as well as polysaccharides. This may be related to the fact that these end branches (the "icicle-like" tips) represent the youngest basidiomatal tissue, in which high amounts of wall components (e.g., chitin and β-glucans) for the differentiating hymenium (incl. basidiospores) has to be synthesized.

For further spectra analysis, principal component analyses were performed to fully characterize the range of spectral variations. With PCA the dimensionality of MIR and NIR microscopic imaging spectra are reduced while as much information as possible is retained. The scores of the first principle components are used to generate meaningful plots without a detailed understanding of the underlying tissue biochemistry.

The results of spectra analyses with PCA of the basal branch, side branches, and end-branches are illustrated in **Fig. 2 (C)-(D)**. The score plot of the first and the second principal component is based on 30 spectra in the MIR region **(C)** and in the NIR region **(D)** of the specimen. For deploying PCA models, reflection spectra were transformed to log (1/*R*). Additional pretreatments for MIR and NIR spectra such as baseline offset and area normalization were utilized. The score plots display a 2-D visualization of spectra clusters for the principal components 1 and 2 explain 80 % of the total variance and can separate the 3 different structure types. PCA models indicate that most of the descriptive information are contained in the region from 3240 cm^{-1} to 750 cm^{-1} (MIR) and in the region from 5300 cm^{-1} to 4000 cm^{-1} (NIR). It is obviously seen in the scores plots that, in general, the black points for the basal branch, the blue points for side branches, and the red points for end branches fall apart. A better separation was achieved in the NIR region, indicating a varying production of polysaccharides. To which extent this variation is caused by qualitative and/or quantitative alterations could not be differentiated.

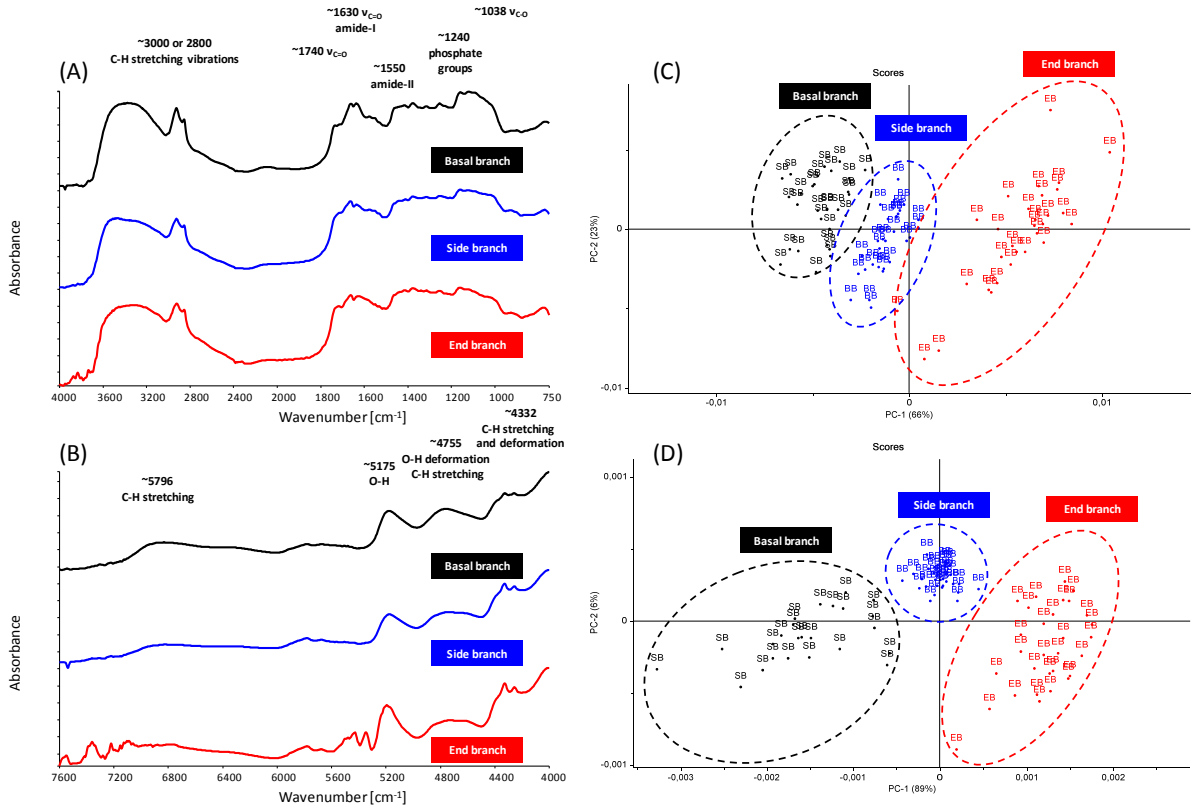

Figure 2 (A)-(B) Typical MIR and NIR spectra of basal branch, side branch, and end-branch regions. Major absorption bands are described in the MIR region. For more specific band assignments see Tab. 1. Score plot of PC1 and PC2 of MIR spectra **(C)** and of NIR spectra **(D)** representation; each colored data point (each sphere) represents one region of interest (ROI) co-registered with the optical scan. This co-registration allows a parallel assessment of histo-anatomical features.

Tab. 1. Assignment of some characteristic bands in the MIR and NIR spectra of basal branch (Bb), side branch (Sb), and end branch (Eb) regions. Upward arrows indicate strong absorption band.

Wavenumber (cm^{-1})	Tentative Assignment	Bb	Sb	Eb
~5796	first overtone of C-H stretching[88]			↑
~5175	O-H stretching and deformation vibration, H_2O, polysaccharides[89, 90]			↑
~4755	first overtone of O-H deformation and C-H stretching[88]	↑	↑	↑
~4332	C-H stretching and deformation combination[88, 91]			↑
~3300	protein amide A vibration[54, 92]	↑	↑	↑
~3000 - 2800	C-H stretching vibrations of phospholipids, of protein side chains, nucleic acid sugars, complex carbohydrates as well as that of amorphous or fully hydrated sugars[51, 61]	↑	↑	↑
~1740	$\nu_{C=O}$ esters, phospholipids as well as carbohydrates[52, 93]			↑
~1630	amide-I proteins[94, 95]	↑		
~1550	amide-II proteins[31, 85]	↑		
~1515	amide-II proteins with high tyrosine content[31, 68, 85]	↑		
~1450-1350	C-H deformation modes and some carboxylic acid modes[31, 68, 85]	↑	↑	↑
~1240	phosphate groups of DNA, RNA as well as some phospholipids[96-98]	↑		
~1185	carbohydrate bands[99]	↑	↑	↑
~1084	$\nu_{P=O}$ symmetric vibrations of the > PO_2^- groups nucleic acids and phospholipids[86, 87, 100]		↑	
~1060	ν_{C-O-C} symmetric vibrations of phospholipids, cholesterols and esters[52]		↑	
~1038	ν_{C-O} carbohydrates[101, 102]			↑

Results presented in **Fig. 3** illustrate the capability of spectroscopic imaging to accurately reproduce 3-D morphology of fungal material. The image displayed in **Fig. 3 (A)** was collected from a *H. coralloides* basidioma measured by MIR and NIR imaging with a nominal lateral resolution of 50 µm × 50 µm per pixel for each spot. The optical image was then directly compared with the images constructed from chemical maps (**Fig. 3 (B)-(D)**). Three histo-anatomical features can be recognized on the optical image: basal branch, side branch, and end branch structures. **Fig. 3 (B)** depicts a 3-D chemical map generated by integrating the area under the band absorption at 1084 cm^{-1}, which is commonly attributed to nucleic acids. This observation indicates that side branch structures are highly proliferating areas.
In contrast, the 3-D chemical map resulting from the absorption at 2956 cm^{-1} (**Fig. 3 (C)**), which is commonly attributed to lipids, proteins, carbohydrates, and nucleic acids, represents a more or less homogeneous distribution over the whole specimen. These observations clearly indicate that the developing hymenial tissue features a generally high metabolic activity.

The 3-D chemical map resulting from the absorption at 4332 cm^{-1} (**Fig. 3 (D)**) represents a higher signal in the end-branch region, which is commonly attributed to polysaccharides. The result correlates well with the morphology/anatomy of the end-branch region: the proportion of hymenial elements (basidioles, basidia, pseudocystidia, and basidiospores) in the “icicle-like” tips is obviously higher than that of the underlying sterile tissue (an accurate quantification was not made). This indicates that this tissue type produces a relatively high amount of polysaccharides like chitin or β-glucans. More specific correlations with morphological and histological features, however, cannot be gauged with this form of processing. Therefore, different cluster analyses were performed to characterize the full range of observed spectral variations.

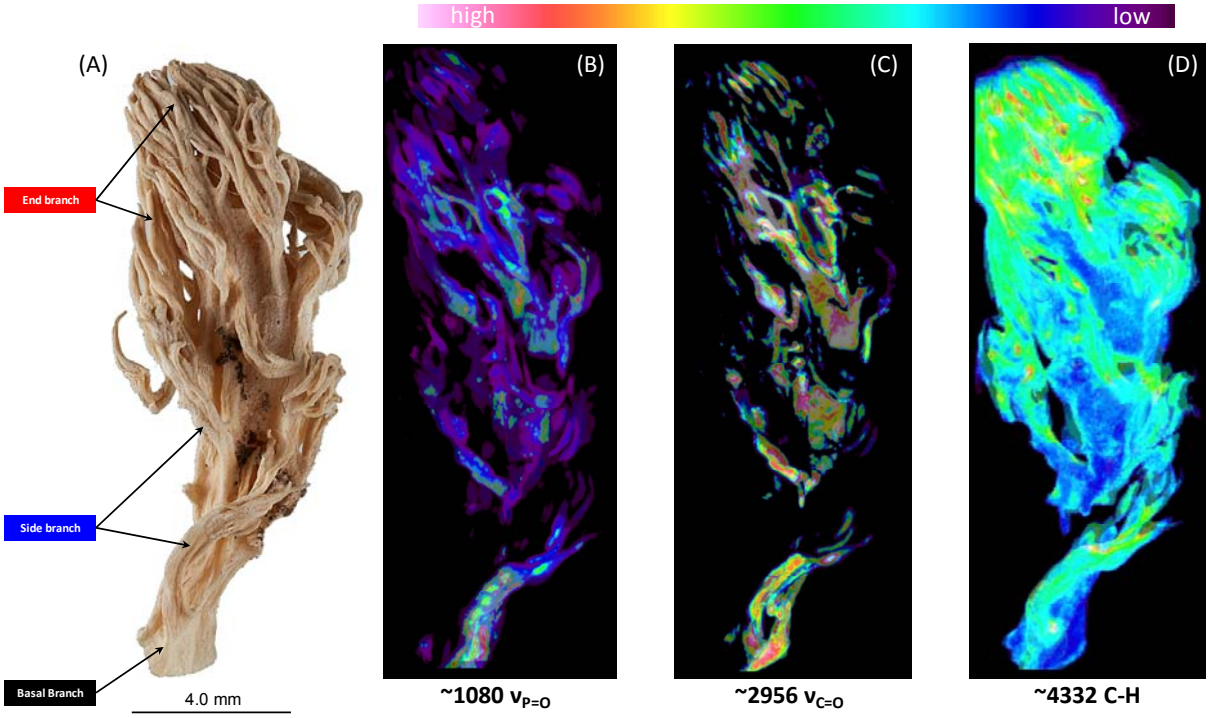

Figure 3 Photograph of a *Hericium coralloides* specimen with marked regions: basal branch, side branch and end branch. **(B)** 3-D surface reconstruction of the imaging result at 1084 cm^{-1}, which is commonly attributed to nucleic acids. **(C)** 3-D surface reconstruction of the imaging result at 2956 cm^{-1}, which points to lipids, proteins, carbohydrates and nucleic acids. **(D)** 3-D surface reconstruction of the imaging result at 4332 cm^{-1} indicates polysaccharides.

Fig. 4 (B) depicts a 3-D pseudo-colour image that was constructed by using HCA. The displayed image represents a five-cluster structure reproducing histo-anatomical features of the measured sample. Green and light blue pixels translate basal branch structures, orange and red pixels encode side branches, blue and pink pixels convert end branches. A 3-D Fuzzy C-means clustering image is displayed in **Fig. 4 (C)**. The principal correspondence between the optical image and the 3-D Fuzzy C-means clustering image is obvious; most of the spectral clusters can be assigned to the histo-anatomical features. **Fig. 4 (D)** illustrates the result of 3-D K-means clustering. Clustering analyses allow a rough assignment to the defined basidioma regions (basal branch, side branches, and end branches), but it should be noted that a more detailed discrimination was not possible so far: further differentiation could not be achieved, even if the number of clusters was increased (data not shown). In our study, it was not possible to check chemical alterations of the fixation and drying process in

comparison with fresh material because no fresh material of this rare fungus was available for the MIR and NIR study at that time. This will be done in a future work.

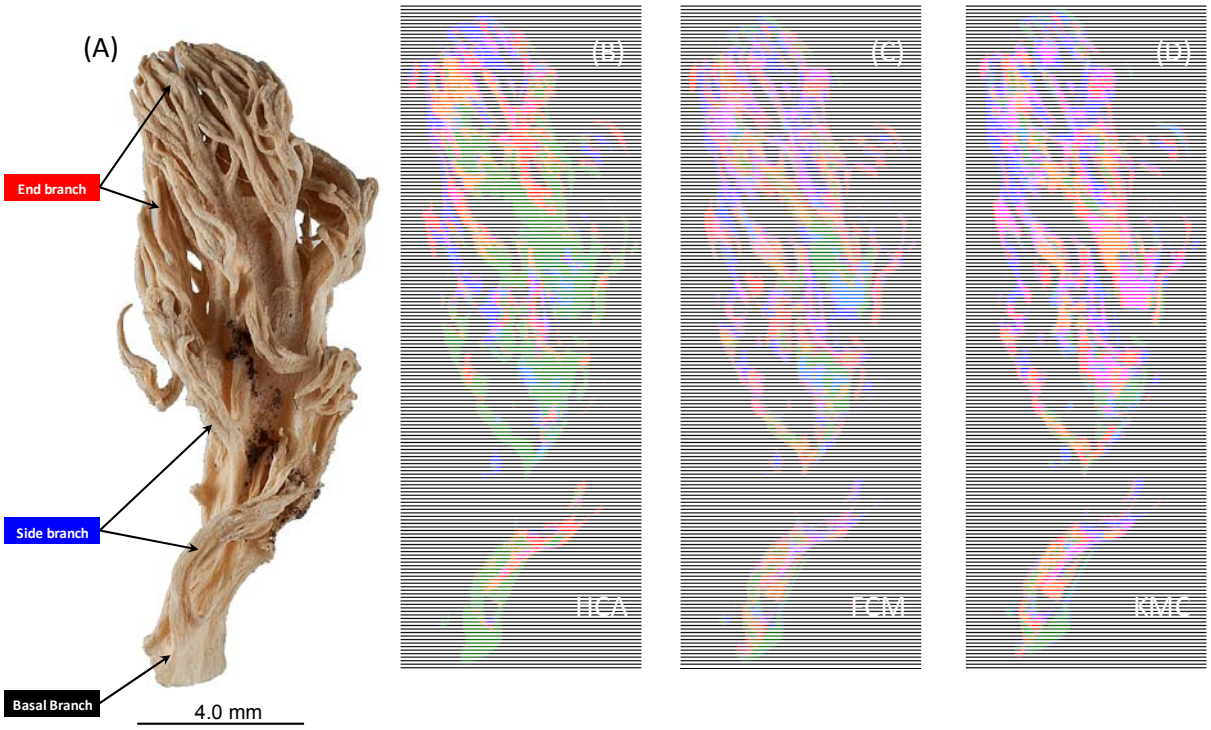

Figure 4 Photograph of a *Hericium coralloides* specimen with marked regions: basal branch, side branches, and end branches. **(B)** 3-D Hierarchical Cluster Analysis. **(C)** 3-D Fuzzy C-means clustering. **(D)** 3-D K-means clustering.

4. Conclusion

In the present study, 3-D MIR and NIR microscopic imaging based on 2-D spectral images acquired from different tissue planes followed by univariate and multivariate data analyses were used to investigate the basidioma (fruiting body) tissue of the potentially medicinal basidiomycete *Hericium coralloides*. We used different clustering techniques (K-means clustering, Fuzzy C-means clustering, and HCA) and proofed that all these clustering algorithms considerably increased the information content of the IR images. For the strongly ramified *H. coralloides* basidioma type [51] we were able to obtain reproducible high quality IR reflection spectra from the basidioma morphology with MIR and NIR microscopic imaging and to semi-quantitatively display the local distribution of substances of certain classes within basidioma structures. Based on histo-chemical properties/information, morphological features of the basidioma can be displayed in false colour representation obtained from an unstained specimen. Specific correlations with morphological traits and discrete chemical compounds, however, cannot be gauged with this form of processing; but, knowing the semi-quantitative distribution of substances of defined classes, such non-destructive techniques might not only be useful for mycological basic research, but also for strain selections as well as quality and safety control in mushroom production.

5. Acknowledgements

The authors would like to thank Prof. Michael Heß from the Histology and Embryology section, Innsbruck Medical University and Christine Pallua for their aid in sample collection and preparation. We also gratefully acknowledge Clemens Unterwurzacher from the Department of Traumatology Innsbruck Medical University for taking basidioma photos and Univ. Prof. Dr. Roland Stalder from the Institute of Mineralogy and Petrography, Leopold-Franzens University for providing the IR microscope. We owe thanks also to Prof. Heinz Siesler from the University of Duisburg-Essen, Germany, and Dipl.-Ing. (FH) Mag. Gregor Mair from the Leopold-Franzens-University of Innsbruck, Austria, for their aid in data analyses.

5. References

1. D. L. Hawksworth, *Mycological Research*, 1991, **95**, 641-655.
2. D. L. Hawksworth, *Mycological Research*, 2001, **105**, 1422-1432.
3. G. M. Cragg, M. R. Boyd, R. Khanna, R. Kneller, T. D. Mays, K. D. Mazan, D. J. Newman and E. A. Sausville, *Pure and Applied Chemistry*, 1999, **71**, 1619-1634.
4. C. Pearce, *Advances in applied microbiology*, 1997, **44**, 1-80.
5. A. Demain, *Applied microbiology and biotechnology*, 1999, **52**, 455-463.
6. P. S. Masurekar, *Biotechnology*, 1992, **21**, 241-301.
7. P. W. Clutterbuck, R. Lovell and H. Raistrick, *Biochem J*, 1932, **26**, 1907-1918.
8. A. Fleming, *Chic Med Sch Q*, 1946, **7**, 20-28.
9. R. S. Fleming and F. B. Queen, *Am J Clin Pathol*, 1946, **16**, 63-65.
10. R. Zocher, T. Nihira, E. Paul, N. Madry, H. Peeters, H. Kleinkauf and U. Keller, *Biochemistry*, 1986, **25**, 550-553.
11. M. Hoppert, C. Gentzsch and K. Schörgendorfer, *Archives of microbiology*, 2001, **176**, 285-293.
12. A. Alberts, J. Chen, G. Kuron, V. Hunt, J. Huff, C. Hoffman, J. Rothrock, M. Lopez, H. Joshua and E. Harris, *Proceedings of the National Academy of Sciences*, 1980, **77**, 3957.
13. R. N. Moore, G. Bigam, J. K. Chan, A. M. Hogg, T. T. Nakashima and J. C. Vederas, *Journal of the American Chemical Society*, 1985, **107**, 3694-3701.
14. N. Gunde-Cimerman and A. Cimerman, *Exp Mycol*, 1995, **19**, 1-6.
15. J. Alarcon, S. Aguila, P. Arancibia-Avila, O. Fuentes, E. Zamorano-Ponce and M. Hernandez, *Z Naturforsch C*, 2003, **58**, 62-64.
16. P. Bobek, L. Ozdin and S. Galbavy, *Nutrition*, 1998, **14**, 282-286.
17. A. Stierle, G. Strobel and D. Stierle, *Science*, 1993, **260**, 214-216.
18. G. Strobel, X. Yang, J. Sears, R. Kramer, R. S. Sidhu and W. Hess, *Microbiology*, 1996, **142**, 435-440.
19. R. S. Chang, V. J. Lotti, R. L. Monaghan, J. Birnbaum, E. O. Stapley, M. A. Goetz, G. Albers-Schonberg, A. A. Patchett, J. M. Liesch, O. D. Hensens and et al., *Science*, 1985, **230**, 177-179.
20. M. A. Goetz, M. Lopez, R. L. Monaghan, R. S. Chang, V. J. Lotti and T. B. Chen, *J Antibiot (Tokyo)*, 1985, **38**, 1633-1637.
21. J. M. Liesch, O. D. Hensens, J. P. Springer, R. S. Chang and V. J. Lotti, *J Antibiot (Tokyo)*, 1985, **38**, 1638-1641.
22. M. G. Bock, R. M. DiPardo, K. E. Rittle, B. E. Evans, R. M. Freidinger, D. F. Veber, R. S. Chang, T. B. Chen, M. E. Keegan and V. J. Lotti, *J Med Chem*, 1986, **29**, 1941-1945.
23. K. Horie, R. Rakwal, M. Hirano, J. Shibato, H. W. Nam, Y. S. Kim, Y. Kouzuma, G. K. Agrawal, Y. Masuo and M. Yonekura, *J Proteome Res*, 2008, **7**, 1819-1835.
24. S. P. Wasser, *Appl Microbiol Biotechnol*, 2011, **89**, 1323-1332.
25. T. Lai, Y. Gao and S. Zhou, *International Journal of Medicinal Mushrooms*, 2004, **6**.
26. U. Lindequist, T. H. Niedermeyer and W. D. Julich, *Evid Based Complement Alternat Med*, 2005, **2**, 285-299.
27. P. Stamets, *Explore (NY)*, 2006, **2**, 152-161.

28. D. I. Abrams, P. Couey, S. B. Shade, M. E. Kelly, N. Kamanu-Elias and P. Stamets, *BMC Complement Altern Med*, 2011, **11**, 60.
29. Z. Wang, D. Luo and Z. Liang, *Carbohydrate Polymers*, 2004, **57**, 241-247.
30. K. Mori, S. Inatomi, K. Ouchi, Y. Azumi and T. Tuchida, *Phytother Res*, 2009, **23**, 367-372.
31. R. Salzer and H. W. Siesler, *Infrared and Raman spectroscopic imaging*, Wiley-Vch, Weinheim, 2009.
32. R. Bhargava and I. Levin, *Spectrochemical analysis using infrared multichannel detectors*, Wiley-Blackwell, 2005.
33. B. R. Wood, K. R. Bambery, C. J. Evans, M. A. Quinn and D. McNaughton, *BMC Med Imaging*, 2006, **6**, 12.
34. H. Ou-Yang, E. P. Paschalis, W. E. Mayo, A. L. Boskey and R. Mendelsohn, *J Bone Miner Res*, 2001, **16**, 893-900.
35. K. Chan and S. G. Kazarian, *Applied spectroscopy*, 2007, **61**, 48-54.
36. T. Frosch, K. A. Chan, H. C. Wong, J. o. T. Cabral and S. G. Kazarian, *Langmuir*, 2010, **26**, 19027-19032.
37. A. G. T. Schut, J. Ketelaars, J. Meuleman, J. G. Kornet and C. Lokhorst, *Imaging spectroscopy for characterisation of grass swards*, 9.
38. C. Yang, J. H. Everitt and C. Mao, A hyperspectral imaging system for agricultural applications, 2001.
39. X. Cheng, Y. R. Chen, Y. Tao, D. Chan and C. Y. Wang.
40. S. Kawamura, M. Natsuga, K. Takekura and K. Itoh, *Computers and Electronics in Agriculture*, 2003, **40**, 115-126.
41. I. Kavdir and D. E. Guyer.
42. H. Hamid Muhammed and A. Larsolle, *Biosystems engineering*, 2003, **86**, 125-134.
43. A. Naumann, M. Navarro-González, S. Peddireddi, U. Kües and A. Polle, *Fungal Genetics and Biology*, 2005, **42**, 829-835.
44. I. Kavdir, R. Lu, D. Ariana and M. Ngouajio, *Postharvest Biology and Technology*, 2007, **44**, 165-174.
45. C. Ridgway, E. Davies, J. Chambers, D. Mason and M. Bateman, *Biosystems engineering*, 2002, **83**, 21-30.
46. C. Ridgway and J. Chambers, *Journal of Near Infrared Spectroscopy*, 1998, **6**, 115-120.
47. C. Ridgway, R. Davies and J. Chambers, Imaging for the high-speed detection of pest insects and other contaminants in cereal grain in transit, 2001.
48. D. Wetzel, *Developments in Food Science*, 1995, **37**, 2039-2108.
49. D. Wetzel, A. Eilert, L. Pietrzak, S. Miller and J. Sweat, *Cellular and molecular biology (Noisy-le-Grand, France)*, 1998, **44**, 145.
50. P. Heraud, S. Caine, G. Sanson, R. Gleadow, B. R. Wood and D. McNaughton, *New Phytologist*, 2007, **173**, 216-225.
51. J. D. Pallua, W. Recheis, R. Poder, K. Pfaller, C. Pezzei, H. Hahn, V. Huck-Pezzei, L. K. Bittner, G. Schaefer, E. Steiner, G. Andre, S. Hutwimmer, S. Felber, A. K. Pallua, A. F. Pallua, G. K. Bonn and C. W. Huck, *Analyst*, 2012, **137**, 1584-1595.
52. V. A. Huck-Pezzei, J. D. Pallua, C. Pezzei, L. K. Bittner, S. A. Schonbichler, G. Abel, M. Popp, G. K. Bonn and C. W. Huck, *Anal Bioanal Chem*, 2012, **404**, 1771-1778.
53. S. F. Chew, B. R. Wood, C. Kanaan, J. Browning, D. MacGregor, I. D. Davis, J. Cebon, B. D. Tait and D. McNaughton, *Tissue Antigens*, 2007, **69 Suppl 1**, 252-258.

54. J. D. Pallua, C. Pezzei, B. Zelger, G. Schaefer, L. K. Bittner, V. A. Huck-Pezzei, S. A. Schoenbichler, H. Hahn, A. Kloss-Brandstaetter, F. Kloss, G. K. Bonn and C. W. Huck, *Analyst*, 2012, **137**, 3965-3974.
55. A. Podshyvalov, R. K. Sahu, S. Mark, K. Kantarovich, H. Guterman, J. Goldstein, R. Jagannathan, S. Argov and S. Mordechai, *Appl Opt*, 2005, **44**, 3725-3734.
56. T. D. Wang, G. Triadafilopoulos, J. M. Crawford, L. R. Dixon, T. Bhandari, P. Sahbaie, S. Friedland, R. Soetikno and C. H. Contag, *Proc Natl Acad Sci U S A*, 2007, **104**, 15864-15869.
57. Q. B. Li, X. J. Sun, Y. Z. Xu, L. M. Yang, Y. F. Zhang, S. F. Weng, J. S. Shi and J. G. Wu, *Clin Chem*, 2005, **51**, 346-350.
58. K. Yano, S. Ohoshima, Y. Gotou, K. Kumaido, T. Moriguchi and H. Katayama, *Anal Biochem*, 2000, **287**, 218-225.
59. C. M. Krishna, G. D. Sockalingum, R. A. Bhat, L. Venteo, P. Kushtagi, M. Pluot and M. Manfait, *Anal Bioanal Chem*, 2007, **387**, 1649-1656.
60. E. Gazi, J. Dwyer, P. Gardner, A. Ghanbari-Siahkali, A. P. Wade, J. Miyan, N. P. Lockyer, J. C. Vickerman, N. W. Clarke, J. H. Shanks, L. J. Scott, C. A. Hart and M. Brown, *J Pathol*, 2003, **201**, 99-108.
61. C. Pezzei, J. D. Pallua, G. Schaefer, C. Seifarth, V. Huck-Pezzei, L. K. Bittner, H. Klocker, G. Bartsch, G. K. Bonn and C. W. Huck, *Mol Biosyst*, 2010, **6**, 2287-2295.
62. D. C. Fernandez, R. Bhargava, S. M. Hewitt and I. W. Levin, *Nat Biotechnol*, 2005, **23**, 469-474.
63. S. Argov, R. K. Sahu, E. Bernshtain, A. Salman, G. Shohat, U. Zelig and S. Mordechai, *Biopolymers*, 2004, **75**, 384-392.
64. C. Krafft, K. Thümmler, S. B. Sobottka, G. Schackert and R. Salzer, *Biopolymers*, 2006, **82**, 301-305.
65. M. Kirsch, G. Schackert, R. Salzer and C. Krafft, *Anal Bioanal Chem*, 2010, **398**, 1707-1713.
66. S. B. Sobottka, K. D. Geiger, R. Salzer, G. Schackert and C. Krafft, *Anal Bioanal Chem*, 2009, **393**, 187-195.
67. M. Kohler, S. Machill, R. Salzer and C. Krafft, *Anal Bioanal Chem*, 2009, **393**, 1513-1520.
68. P. Lasch and J. Kneipp, *Biomedical vibrational spectroscopy*, Wiley. com, 2008.
69. B. Bird, M. Miljkovic, M. J. Romeo, J. Smith, N. Stone, M. W. George and M. Diem, *BMC Clin Pathol*, 2008, **8**, 8.
70. C. Gendrin, Y. Roggo and C. Collet, *Journal of pharmaceutical and biomedical analysis*, 2008, **48**, 533-553.
71. P. Geladi, *Techniques and applications of hyperspectral image analysis*, Wiley, 2007.
72. P. Lasch, W. Haensch, D. Naumann and M. Diem, *Biochim Biophys Acta*, 2004, **1688**, 176-186.
73. R. Dell'Anna, P. Lazzeri, M. Frisanco, F. Monti, F. Malvezzi Campeggi, E. Gottardini and M. Bersani, *Anal Bioanal Chem*, 2009, **394**, 1443-1452.
74. E. Ly, O. Piot, R. Wolthuis, A. Durlach, P. Bernard and M. Manfait, *Analyst*, 2008, **133**, 197-205.
75. J. Guilment, S. Markel and W. Windig, *Applied spectroscopy*, 1994, **48**, 320-326.

76. J. D Pallua, C. Pezzei, V. Huck-Pezzei, S. A Schonbichler, L. K Bittner, G. K Bonn, A. Saeed, S. Majeed, A. Farooq and M. Najam-ul-Haq, *Current Bioactive Compounds*, 2011, **7**, 106-117.
77. J. D Pallua, C. Pezzei, G. Schaefer, B. Zelger, A. Brunner, A. Kloss-Brandstaetter, F. Kloss, H. Klocker, G. Bartsch and V. A Huck-Pezzei, *Current Proteomics*, 2012, **9**, 132-142.
78. P. Lasch and D. Naumann, *Cell Mol Biol (Noisy-le-grand)*, 1998, **44**, 189-202.
79. P. Y. Wei, H. Q. Pu, X. Wei, C. G. Li and S. Nong, *Zhong Yao Cai*, 2007, **30**, 1270-1273.
80. C. P. Schultz and H. H. Mantsch, *Cell Mol Biol (Noisy-le-grand)*, 1998, **44**, 203-210.
81. M. Jackson, B. Ramjiawan, M. Hewko and H. H. Mantsch, *Cell Mol Biol (Noisy-le-grand)*, 1998, **44**, 89-98.
82. M. Diem, L. Chiriboga and H. Yee, *Biopolymers*, 2000, **57**, 282-290.
83. L. Zhang, G. W. Small, A. S. Haka, L. H. Kidder and E. N. Lewis, *Appl Spectrosc*, 2003, **57**, 14-22.
84. J. R. Mansfield, M. G. Sowa, G. B. Scarth, R. L. Somorjai and H. H. Mantsch, *Comput Med Imaging Graph*, 1997, **21**, 299-308.
85. R. Bhargava and I. Levin, *Spectrochemical analysis using infrared multichannel detectors*, Wiley-Blackwell, 2006.
86. M. J. Walsh, T. G. Fellous, A. Hammiche, W. R. Lin, N. J. Fullwood, O. Grude, F. Bahrami, J. M. Nicholson, M. Cotte, J. Susini, H. M. Pollock, M. Brittan, P. L. Martin-Hirsch, M. R. Alison and F. L. Martin, *Stem Cells*, 2008, **26**, 108-118.
87. J. G. Kelly, T. Nakamura, S. Kinoshita, N. J. Fullwood and F. L. Martin, *Analyst*, 2010, **135**, 3120-3125.
88. J. S. Shenk, J. Workman and M. O. Westerhaus, *PRACTICAL SPECTROSCOPY SERIES*, 2001, **27**, 419-474.
89. P. Vasko, J. Blackwell and J. Koenig, *Carbohydrate Research*, 1972, **23**, 407-416.
90. P. D. Vasko, J. Blackwell and J. Koenig, *Carbohydrate Research*, 1971, **19**, 297-310.
91. F. Barton and D. Himmelsbach, *Applied spectroscopy*, 1993, **47**, 1920-1925.
92. L. H. Kidder, P. Colarusso, S. A. Stewart, I. W. Levin, N. M. Appel, D. S. Lester, P. G. Pentchev and E. N. Lewis, *Journal of Biomedical Optics*, 1999, **4**, 7-13.
93. K. Stehfest, J. Toepel and C. Wilhelm, *Plant Physiology and Biochemistry*, 2005, **43**, 717-726.
94. H. H. Mantsch and D. Chapman, *Infrared spectroscopy of biomolecules*, Wiley-Liss, 1996.
95. H.-U. Gremlich and B. Yan, *Infrared and Raman spectroscopy of biological materials*, CRC Press, 2001.
96. P. Wong, E. Papavassiliou and B. Rigas, *Applied spectroscopy*, 1991, **45**, 1563-1567.
97. J. Legal, M. Manfait and T. Theophanides, *Journal of molecular structure*, 1991, **242**, 397-407.
98. J. Kneipp, M. Beekes, P. Lasch and D. Naumann, *The Journal of neuroscience*, 2002, **22**, 2989-2997.
99. J. J. van Soest, H. Tournois, D. de Wit and J. F. Vliegenthart, *Carbohydrate Research*, 1995, **279**, 201-214.
100. P. Lasch, M. Boese, A. Pacifico and M. Diem, *Vibrational spectroscopy*, 2002, **28**, 147-157.

101. N. B. Colthup, L. H. Daly and S. E. Wiberley, *Introduction to infrared and Raman spectroscopy*, Academic press, 1990.
102. D. Lin-Vien, N. B. Colthup, W. G. Fateley and J. G. Grasselli, *The handbook of infrared and Raman characteristic frequencies of organic molecules*, Academic Press, 1991.